Electrochemistry at Conductor/Insulator/Electrolyte Three-Phase Interlines: A Thin Layer Model

Yuan Deng,[†] Dihua Wang,*[,†] Wei Xiao,[†] Xianbo Jin,[†] Xiaohong Hu,[†] and George Z. Chen*[,†,‡]

College of Chemistry and Molecular Sciences, Wuhan University, Wuhan 430072, People's Republic of China, and School of Chemical, Environmental and Mining Engineering, University of Nottingham, Nottingham NG7 2RD, U.K.

Received: November 26, 2004; In Final Form: May 23, 2005

A thin layer model is proposed to assist in the understanding of the electrochemical conversion of insulator to conductor at the conductor/insulator/electrolyte three-phase interline (3PI) when the influence of mass diffusion in the electrolyte phase is negligible. The model predicts, under potentiostatic conditions, a linear variation of the current or the length of the 3PI with time. When polarization is sufficiently large, the logarithm of the current/time ratio or the 3PI-length/time ratio, according to the model, increases linearly with the applied potential. These predictions were tested against and agreed very well with two practical systems: the electroreduction of solid AgCl to Ag in aqueous KCl and of solid SiO_2 to Si in molten $CaCl_2$. Kinetic parameters were derived from experimental data using the model. Particularly, the electron transfer coefficient, α, was found to be about 0.29 for the reduction of AgCl to Ag in the aqueous KCl solution at room temperature but about 10^{-2} for the reduction of SiO_2 to Si in molten $CaCl_2$ at 850 °C.

Introduction

Over the past half of a century, the majority of electrochemical studies and applications have focused on the structure of and process at the two-phase interface between an electron conductor (electrode) and an ion conductor (electrolyte).[1] Accordingly, the dominant theory of electrochemistry and related research methodologies have been established and developed on the basis of observations and understanding of the phenomena and kinetics at electrified interfaces.[2] However, many electrochemical processes involve three phases. Typical examples include (1) the solid (electrode and catalyst)/solid (polymer or solid oxide electrolyte)/gas (oxygen or hydrogen) three-phase regions or boundaries in the polymer membrane electrolyte or solid oxide fuel cells[3−10] and sensors,[11,12] (2) the solid (electrode)/liquid (oil)/liquid (aqueous electrolyte) three-phase boundaries in the electrochemical investigation of the liquid/liquid interface,[13−16] and (3) the solid (electrode and catalyst)/liquid (aqueous or organic electrolyte)/gas (CO_2 or vapor of MeOH) three-phase boundaries in the reduction of gases.[17,18] The solid/solid/gas systems are perhaps mostly investigated due to their importance in fuel cells. More recently, studies of the solid/liquid/liquid systems have been greatly facilitated by the use of an organic droplet (either redox active[19,20] or containing the redox active compound[21−23]) on a planar electrode surrounded by an aqueous electrolyte. In particular, the employment of an additional microelectrode to probe into the organic droplet can greatly assist in the accurate identification of the three-phase reaction zones.[22] A relatively less reported case in the literature is the solid/solid/liquid three-phase systems which also apply to many important electrochemical devices and techniques, as well exemplified in the solid (Pb or PbO_2)/solid ($PbSO_4$)/liquid (H_2SO_4 and H_2O) three-phase reaction regions involved in the lead−acid secondary batteries.[24] A new development of the solid (conductor)/solid (oxide or compound)/liquid (molten salt) three-phase electrochemistry involves the direct extraction of titanium, silicon, or chromium from the respective solid oxides in molten calcium chloride.[25−28] This new work has drawn increasing global attention from both academia and industry.[29−31] Particularly, the dynamic nature or propagation of the three-phase boundaries may lay a foundation for understanding and application of the new process.

Traditionally, the term three-phase boundary (TPB) is often used[3−16] and possibly originates from the solid oxide fuel cell study. Occasionally, a more confusing term, three-phase interface,[16,17,26,32] also appears in some literature. Geometrically, what connects two phases is a two-dimensional face (flat or uneven plane) but what connects three phases is a one-dimensional line (straight or curved). In analogy to the well-known phrase two-phase interface, the concept of the *three-phase interline* comes naturally and was actually used previously in some non-electrochemical fields[33,34] and recently recognized by electrochemists.[28,35,36] It should be pointed out that the connection of three phases can also be realized at a point if one of the three phases has a sharp end point in contact with the others. Furthermore, an interface can only connect two phases but an *interline* or *interpoint* can join more than three phases. In this paper, only the three-phase interlines (3PIs) are discussed. Finally, the authors are convinced that the separate expressions of an interline and its immediate neighboring three phases can have the same effect as the separate expressions of an interface and its immediate neighboring two phases.

A comparison between the 3PIs in the various above-mentioned examples reveals a difference: with the continuation of the electrochemical reactions, the 3PI remains unchanged with a fixed length in fuel cells and sensors (*disregarding variations at the atomic or molecular level*) but moves with a variable length in the two latter examples of the lead−acid battery and the electroreduction of solid oxides because of the

* To whom correspondence should be addressed. E-mail: george.chen@nottingham.ac.uk (G.Z.C.); dhwang@mail.edu.cn (D.W.).

[†] Wuhan University.

[‡] University of Nottingham.

10.1021/jp044604r CCC: $30.25
Published on Web 07/06/2005

electrochemically driven conversion between the two solid phases. In other words, the 3PI is *stationary* in the former but *dynamic* in the latter. Largely due to the historical and current interest in fuel cells, stationary 3PIs have been intensively investigated.[3−12] However, it is only in recent years that attention has been being directed to dynamic 3PIs. At room temperature, atomic force microscopy was successfully used to investigate (1) the electrochemical reduction of silver and mercury halides and lead oxide and (2) the electrochemical oxidation of white phosphorus at the three-phase junction lines of the nanometer to sub-micrometer scales.[36−38] This technique still needs more development for the electrochemical reduction of solid oxides to the respective metals and alloys in high temperature molten salts,[25−28,35] whereas understanding of the new process is urgently needed by the industry for theoretical guidance in designing an efficient cathode for the electroreduction of solid metal oxides to metals and alloys.[29−31]

This paper reports the first set of results from our ongoing research program aiming at understanding 3PI electrochemistry under various circumstances. These include studying relatively simple 3PI systems that involve a metal or semimetal (solid electron conductor), the metal's compound (solid electron insulator), and an electrolyte (liquid ion conductor). In such a system, the 3PI grows from a point or small circle into a larger circle in the absence of or negligible influences from mass diffusion. Particularly, the 3PI movement, which results purely from the electrochemical conversion between the two solid phases, is confined in a thin layer that may be considered as a pseudo-two-dimensional flat plane. In accordance with the model, a novel experimental setup was designed and used to enable visual observation of the electrochemically driven 3PI movement under different conditions. The classic reduction of AgCl to Ag in aqueous solution[36] and the newly reported reduction of SiO_2 to Si in molten $CaCl_2$[26,27] were employed to test the thin layer model. Cyclic voltammetry and chronoamperometry were performed to obtain data that can be correlated with the theoretical predictions.

Principle

Stationary 3PI. This type refers to a 3PI that is immobile beyond the atomic or molecular scales, and it is the same as that which exists in the polymer membrane electrolyte and solid oxide fuel cells (PEMFC and SOFC) and also in some electrochemical sensors mentioned in the Introduction section. Studies on stationary 3PIs are well documented in the literature[3−18] and will not be discussed in this paper.

Dynamic 3PI. As mentioned above, the 3PIs in the lead−acid battery and in the electroreduction of solid metal compounds (e.g., oxides and halides) are mobile with a variable length that changes with the continuation of the electrochemical process. The dynamic nature of such 3PIs results from the conversion between the two solid phases. For example, in the solid oxide case, the reduction begins at the 3PI of the current collector (metal), oxide, and molten salt and converts the solid oxide in direct contact with the current collector to the metal. At the same time, the charge balancing component, that is, oxygen, in the oxide is ionized and enters the electrolyte. Therefore, further reduction of the compound can proceed at the 3PI linking the newly formed metal with the neighboring oxide and electrolyte, leading to a continuous movement of the 3PI. The removal of oxygen can lead to a volume reduction of the solid phase, which means a likely porous structure in the produced metal if the atomic movement is relatively slow. The porous structure of the metal allows further access by electrolyte to the interior of the solid phase, which allows further propagation of the 3PI not only along the surface but also into the inner part of the solid.[27]

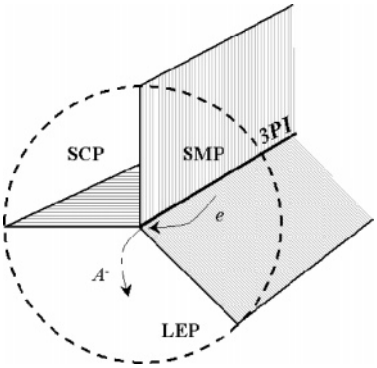

Figure 1. Schematic representation of a three-phase interline (3PI) connecting a solid metal phase (SMP), a solid compound phase (SCP), and a liquid electrolyte phase (LEP). The shaded areas are the interfaces between two neighboring phases. On the 3PI, electron transfer occurs between SMP and SCP and anion transfer takes place between SCP and LEP.

In analogy to the interface whose area determines the overall rate of the electrode reaction, a longer 3PI also means a larger current flow. Similarly, the current density along the 3PI should be a function of the electrode potential. However, because of the dynamic nature of the 3PI, the relationship between the overall current and the applied potential may not be the same as in the case of a stationary interface. Obviously, understanding how the 3PI changes under different working conditions is crucial for the prediction of, for example, the speed and completion of the electroreduction of a solid metal compound to the metal and also the charge−discharge kinetics in batteries.

Simplified Case of the Dynamic 3PI. This is shown in Figure 1 in which the 3PI joins (1) a solid compound phase (SCP) which is electronically insulating but electrochemically active, (2) a solid metal phase (SMP) of good electrochemical inertness, and (3) a liquid electrolyte phase (LEP) which is capable of transporting substances or ions resulting from the electrochemical conversion between the two solid phases. Further, in the system, (4) electron transfer occurs only between the SCP and the SMP at the 3PI and results in conversion between the two solid phases, accompanied by mass transfer between the SCP and the LEP to maintain electric neutrality in the solid phases; (5) both the SCP and the SMP are insoluble or negligibly soluble in the LEP, and the LEP contains no (or negligible) electrochemically active species other than that exchangeable with the SCP.

Practical 3PI systems satisfying the above definitions are plentiful, but two of these are worth mentioning. The first is the recently reported electroreduction of solid silica (plate or powder) to silicon in molten calcium chloride.[26,27]

$$SiO_2\ (SCP) + 4e \rightleftharpoons Si\ (SMP) + 2O^{2-}\ (LEP) \qquad (I)$$

The interest in reaction I is the possibility of the elimination or decrease of the use of carbon from the silicon production industry without compromising product quality and energy consumption.[27] The second example exists in the classic Ag/AgCl/KCl reference electrode.

$$AgCl\ (SCP) + e \rightleftharpoons Ag\ (SMP) + Cl^-\ (LEP) \qquad (II)$$

The differences between the two systems are the reaction temperature and the concentration of the ionized species in the

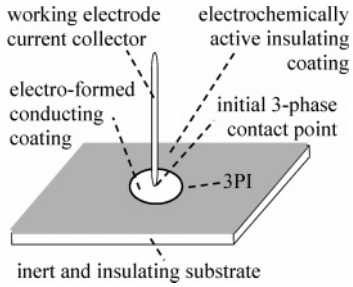

Figure 2. Schematic representation of the thin layer model for the investigation of the electrochemistry at the conductor/insulator/electrolyte three-phase interline (3PI).

LEP. For SiO_2 reduction, the molten salt is at high temperatures (500−900 °C)[26,27] and is required to contain as little as possible of the oxygen ion, while a relatively high chloride concentration is needed for the Ag/AgCl reference electrode to export a stable potential at room temperature. Because AgCl is insoluble in water (solubility product: $K_{sp}(25\ °C) = 1.8 \times 10^{-10}$), a chloride salt such as KCl is added to the solution. (The Ag/AgCl reference electrode can also be used in high temperature molten salts, but in such cases, the AgCl is not a solid but dissolves in the melt[39]). As for the study of 3PI electrochemistry, reaction II is our first choice for experimental simplicity and convenience.

Thin Layer Model. In a practical system represented by reaction I or II, the 3PI movement is often multidirectional in a three-dimensional space. There may also exist more than one 3PI if there are initially multiple SCP−SMP contacts. During the course of movement, the 3PI may encounter another 3PI, which can either force changes in the movement direction of the two 3PIs or simply terminate their movements. The rate determining step(s) of the 3PI movement can be very different and highly case dependent, which makes it a challenge to model the reality comprehensively.

To simplify the situation, one may consider a very thin and porous film of the solid compound phase (SCP, insulating and electrochemically active) that is either free-standing or supported on an insulating and electrochemically inert substrate. The film thickness is so small that mass transfer between the SCP and the liquid electrolyte phase (LEP) and mass transport (diffusion) within the porous SCP impose effectively no influence. Furthermore, one can make the solid metal phase (SMP) into a pin that is placed on top of the SCP film. With the progress of the electrochemical reaction, the SCP at the contact region is converted to the SMP, and the 3PI expands radially along the SCP/LEP interface. Under the given conditions, the reaction rate should only be related to the number of reaction sites along the 3PI (or the length of the 3PI).

Figure 2 shows schematically a setup in accordance with the above simplification. It is acknowledged that this setup resembles, in principle, what was reported recently for the "pinpoint reduction" of silica glass to silicon in molten $CaCl_2$.[26] The differences are that in our case the SCP, SMP, and LEP are AgCl, Ag, and aqueous KCl, respectively and the initial SCP is porous. Also, the 3PI movement is more confined within a thin layer or pseudo-two-dimensional plane. According to Faraday's law, at a given potential for a reduction process, for example, reaction II, the amount of charge transferred is in direct proportion to the quantity of reduced material within a given time. For a coating with a thickness of h, if one assumes (1) a constant line current density, i, along the 3PI at an applied constant potential, (2) a fixed number, m, of parallel planes under the surface, which is equivalent to the 3PI having a reaction zone of h/m in "thickness" or "diameter" surrounding the atoms along the 3PI, and (3) each plane has only one 3PI, the application of Faraday's law to Figure 2 leads to the following equation:

$$\int_0^t i\pi D(t)m\ \mathrm{d}t = \frac{\pi\left(\frac{D(t)}{2}\right)^2 h\rho}{M} nF \tag{1}$$

where $D(t)$ and $\pi D(t)$ are respectively the time dependent diameter and circumference of the circular 3PI, M is the molar mass of AgCl, h and ρ are respectively the thickness and apparent density of the porous AgCl coating on the glass plate, and n and F are respectively the number of electrons transferred and the Faraday constant. Equation 1 is based on the assumption that the 3PI in each plane has the same length and varies at the same speed and direction in length. Differentiation of both sides of eq 1 with respective to time, t, leads to

$$\frac{\mathrm{d}D(t)}{\mathrm{d}t} = V_D = \frac{2mMi}{hnF\rho} \tag{2}$$

Integration of eq 2 gives the following linear relation between $D(t)$ and t.

$$D(t) = \frac{2mMi}{hnF\rho} t = V_D t \tag{3}$$

Equations 2 and 3 indicate that the diameter of the 3PI grows proportionally with the time, meaning a constant rate, $\mathrm{d}D(t)/\mathrm{d}t = V_D$, which is determined by the electrode reactions (n, i) and also the properties of the SCP (h, ρ, m, M). Since the total current on each 3PI is $i\pi D(t) = i\pi V_D t$ and there are m planes (3PIs), the measurable current, I, can be expressed as $I = im\pi V_D t$. Combining this expression with eqs 2 or 3 leads to eq 4.

$$I = \frac{2\pi m^2 M}{hnF\rho} i^2 t = \frac{\pi hnF\rho}{2M} V_D{}^2 t \tag{4}$$

Equation 4 indicates that the total current, which is measurable, is proportional to the time, t. The relationship of the current density, i, with the 3PI growth rate, V_D, from eq 3, or with the current variation rate, $I/t = V_I$, from eq 4, can also be derived.

$$i = \frac{hnF\rho}{2mM} V_D \tag{5}$$

$$i = \sqrt{\frac{hnF\rho}{2\pi m^2 M}} \sqrt{V_I} \tag{6}$$

At a sufficiently large overpotential, $\eta = |E - E^\circ|$, $i = i_0 \exp[(\alpha nF/RT)\eta]$, where E and E° are the applied and equilibrium potentials, respectively; i_0 is the exchange line current density with reference to the 3PI; α is the charge transfer coefficient; R is the gas constant; and T is the temperature. Equations 5 and 6 can be rewritten in the following linear forms.

$$\ln|V_D| = \ln\left(\frac{2mM}{hnF\rho} i_0\right) + \frac{\alpha nF}{RT}\eta \tag{7}$$

$$\ln|V_I| = \ln\left(\frac{2\pi m^2 M}{hnF\rho} i_0{}^2\right) + \frac{2\alpha nF}{RT}\eta \tag{8}$$

Since both V_D and V_I are experimentally measurable, eqs 7 and 8 predict their semilogarithm variations with the applied overpotential. Also, from the slopes of these straight lines can be derived the values of important electrochemical parameters,

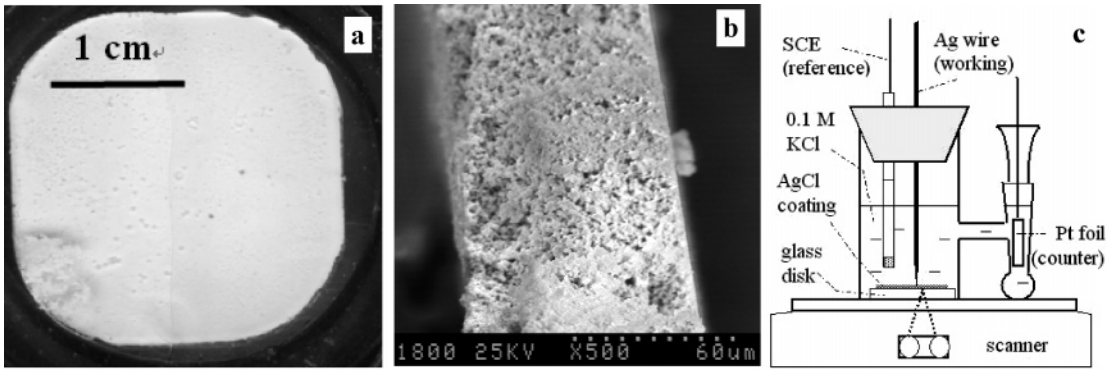

Figure 3. Optical image of the top view of a thin AgCl coating on a glass disk (a) and the SEM image of the cross section of the coating (b). In part c is shown schematically the experimental setup for the investigation of the electroreduction of AgCl to Ag at the Ag/AgCl/(KCl + H_2O) three-phase interline.

for example, the product, αn, of the charge transfer coefficient, α, and the number of transferred electrons, n. Further, as the thickness and apparent density of the film can both be measured or the product of $h\rho$ can be derived from eq 4, the value of mi_0 or mi_0/h can be obtained from the intercept of eqs 7 or 8, which resembles the "current density" (area) through the cross section of the thin layer.

It should be pointed out that the thin layer model described above does not take some other possibilities into consideration. For example, (1) mass (e.g., ion) transfer may occur in one of the two solid phases or through the boundary between the same or different particles, and (2) electrons are likely conducted through an intermediate product phase. Both would encourage the formation of "interphases" and shift the reaction zones from interlines to interfaces.[40] Such systems were considered in the literature.[21−23,36−38]

Experimental Section

Preparation of the AgCl Coating on Glass. The aqueous solution of 0.4 M $AgNO_3$ (15 mL) was added dropwise into the 0.2 M KCl aqueous solution (50 mL) under ultrasonication. After filtration under low pressure and washing with water, the wet white sediment was mixed with 1.5 mL of 10 wt % carboxymethylcellulose (CMC, as the binder) solution into a slurry. A few drops of the slurry were dripped onto the surface of a thin glass disk (2 mm thickness, 30 mm diameter). A thin and fully stretched cotton thread was used to spread the slurry drops into a smooth and uniform coating. After being left in air under darkness for more than 15 h, the coating was dried and remained coherently on the glass disk; see Figure 3a. A small piece of the dried coating was pealed off the glass plate and its cross section inspected under a scanning electron microscope (SEM). A typical SEM image of the cross section of the AgCl coating is shown in Figure 3b. It is acknowledged that the nature of manual operation means a limited control in the preparation of the coating, but the accurate thickness of the coating can be determined by, for example, SEM, as displayed in Figure 3b from which it can be seen that the coating was porous with a satisfactory uniform thickness of about 80 μm.

Simultaneous Electrochemical and Photographic Measurements. The coated glass disk was, with the coating facing upward, placed at the bottom of a two-compartment cell made of glass. The working and counter electrode compartments were arranged in the "H" shape and connected by a glass tube with a frit separator. The internal diameter of the working electrode compartment was 38 mm. The H-cell was placed on top of an optical image scanner which was used to record the color change of the AgCl coating during electrochemical measurements.

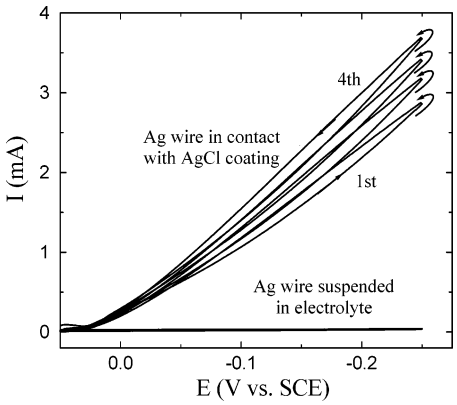

Figure 4. Consecutive cyclic voltammograms in 0.1 M KCl of a silver wire that was suspended in the electrolyte or in contact with a porous AgCl coating on glass (see Figure 3 for the cell setup). The arrows indicate the direction of current variation with the potential scan. Scan rate: 10 mV/s.

Figure 3c illustrates the cell setup in detail. The 500 μm silver wire had a sharp lower end. It was suspended either in the solution or in contact with the AgCl coating for recording cyclic voltammograms.

It should be mentioned that the image taken by the scanner was the coating's back that was in touch with the glass plate. Also, there was a time gap for the light beam to scan between different points of the image, which increased with increasing resolution of the image. In this work, the resolution was set to 2400*4800 dpi. It was found that the current was interrupted when the light beam moved over the reaction area. The interruption usually lasted for less than 1 s but could reach up to 2 s at large polarizing electrode potentials for AgCl reduction and/or high resolution scanning. As will be shown later in this paper, the change within such a short time was too small to cause noticeable errors in the results. Finally, in the experiments, the H-cell was wrapped with black paper to avoid decomposition of the AgCl coating by the natural light. Again, the influence of the light beam from the scanner was proven to be insignificant.

All experiments on the electroreduction of solid AgCl were conducted under ambient conditions. The SiO_2 reduction was carried out in molten $CaCl_2$, as described elsewhere.[27,42]

Instrumentation and Chemicals. The Uniscan C800 color scanner (Tsinghua Unisplendor Co. Ltd., China) was used for optical imaging. Electrochemical data were recorded on a computer controlled CHI660A electrochemical system (Shanghai Chenghua, China). Microscopy was performed on a Hitachi x-650 scanning electron microscope (SEM) that was equipped

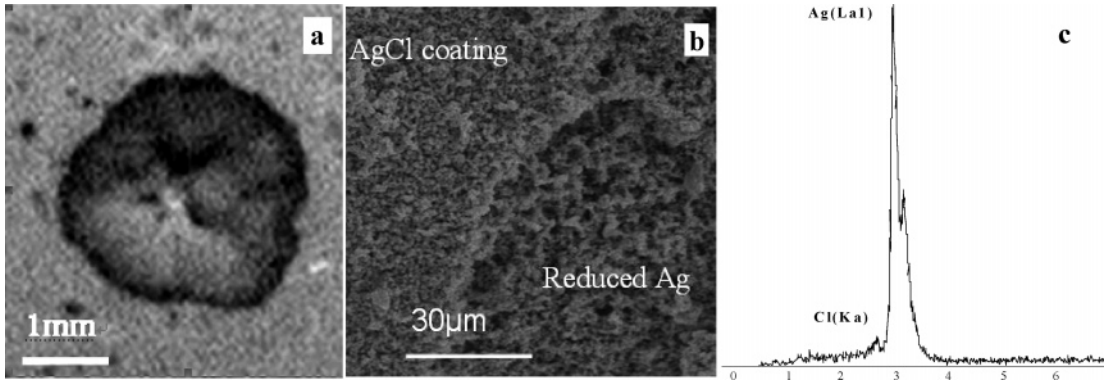

Figure 5. Scanning optical (a) and electron microscopic (b) images of the Ag/AgCl coating, showing the electroreduced regions in the coating. In part c is shown the spectrum of EDX analysis of the reduced region in part b.

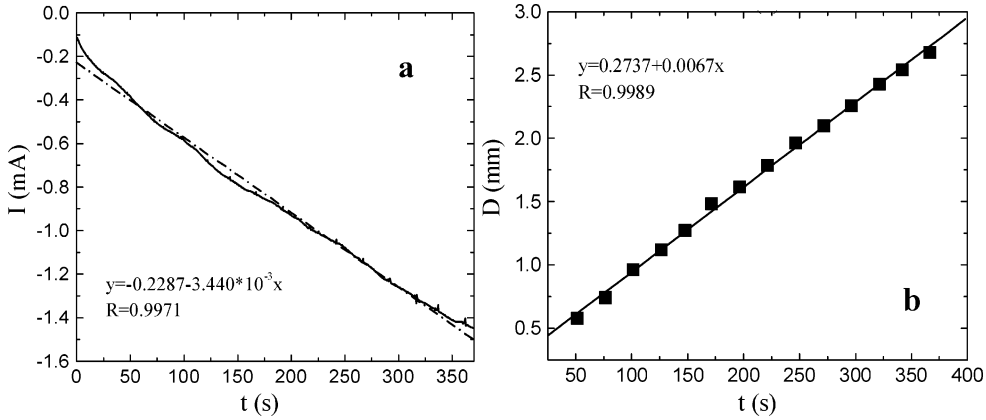

Figure 6. Correlations of (a) the current and (b) the diameter of the 3PI with the time of electrolysis at −0.2 V vs SCE.

with energy dispersive X-ray (EDX) analysis (Japan). All chemicals were of AnalaR grade. Double distilled water was used for making all solutions.

Results and Discussion

Cyclic Voltammetry. Figure 4 shows the consecutive cyclic voltammograms (CVs) recorded using the cell illustrated in Figure 3c with the silver wire's tip being or not being in contact with the AgCl coating. Very small currents were recorded when the silver wire was suspended in the solution and the potential was scanned between 0.1 and −0.25 V where silver should be electrochemically inert at negative potentials but dissolve near the anodic end (the oxidation currents were too small to be seen on the CVs). When the wire tip touched the AgCl coating, increasing currents were recorded with scanning negatively the potential. These reduction currents must have resulted from the reduction of the AgCl coating (otherwise, they should have been seen when the wire was suspended in the electrolyte). In addition, the following features can been seen on the CVs. (1) The current increased almost linearly with the potential without showing any diffusion limited behavior at potentials much more negative than the equilibrium potential of reaction ($E° = 0.03$ V vs SCE in 0.1 M KCl). (2) During each potential cycle, the currents were greater of the reversed (positive) scan than of the forward (negative) scan. (3) The overall CV currents increased with continuous cycling of the potential. To our knowledge, such CV features were not reported in previous literature but are expected according to the 3PI electrochemistry as explained below.

At intervals and after recording the CVs, images of the back of the AgCl coating (in contact with the glass disk) were recorded by the optical scanner, showing a gray/black and approximately circular area growing around the wire tip with potential cycling. In addition, the circular area was found to be more porous than the unreduced area, obviously due to the removal of the large Cl^- ions from the AgCl coating within the circular area. SEM and EDX analyses confirmed the circular gray area to be pure Ag. A minute amount of Cl (<0.5 wt %) was also detected in the circular area by EDX, likely due to contamination by the Cl^- rich environment. Figure 5 presents typical examples of the optical and SEM images and also an EDX spectrum of the circular area in the coating, supporting the CVs of Figure 4 to be indeed originated from reaction II. These findings provide a qualitative account of the CV features (2) and (3) of Figure 4; that is, the current increase with the number of potential cycles was due to the continuous expansion of the circular Ag/AgCl/electrolyte 3PI with both potential and time, as predicted by eqs 4 and 8.

It should be pointed out that because the CV currents resulted from the simultaneous contribution from both time and potential, a comprehensive and more quantitative account goes beyond the application range of eqs 1−8 which however should be more applicable to potential step experiments or chronoamperometry.

Chronoamperometry. Equations 1−8 of the thin layer model assume a constant and significant polarization potential, E, from the equilibrium potential, $E°$, which for reaction II is 0.03 V versus SCE in 0.1 M KCl. Therefore, chronoamperometry was performed at potentials so that $(E° - E) > 150$ mV.

A typical current−time plot recorded at −0.20 V is presented in Figure 6a. Clearly, except for the first 40 s, the current varies linearly with time, as expected from eq 4. The initial deviation from the linear relationship could be related to the non-negligible thickness of the coating (50−80 μm). Logically, during reduction, the 3PI propagation would experience two different stages,

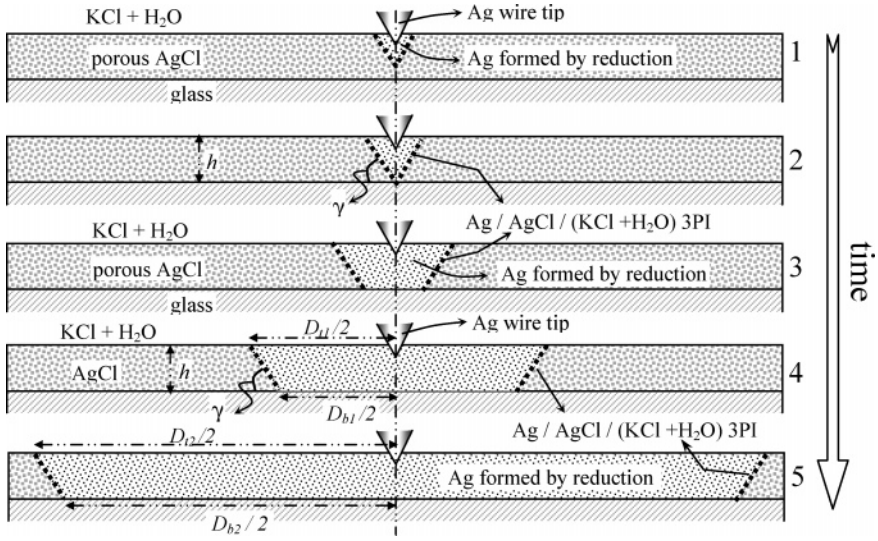

Figure 7. Schematic illustrations of the outward propagation of the Ag/AgCl/(KCl + H_2O) 3PI from around the silver wire tip in contact with a thin AgCl coating on glass. Note that the removal of the large chloride ion may either decrease the layer thickness of the reduced region or form a more porous structure. In this work, it was observed that the Ag region was indeed more porous than the AgCl regions, as shown in Figure 5b, which forms the basis for the same thickness of the AgCl and Ag layers depicted in these drawings.

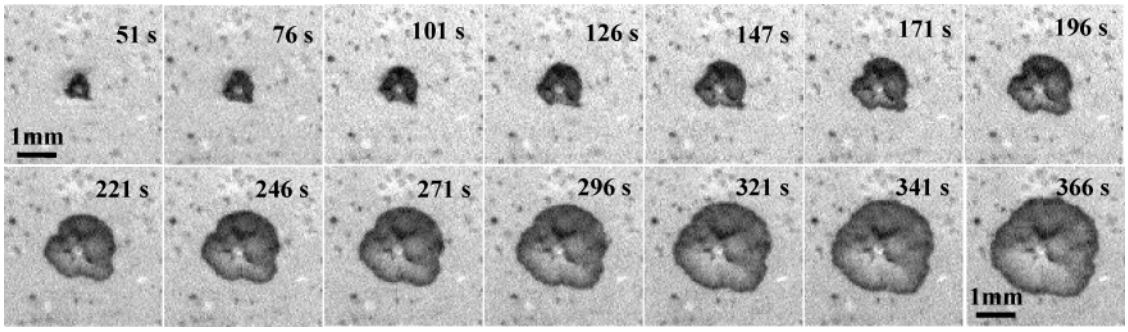

Figure 8. Scanning optical images of the reduced area on the AgCl coating at different times of constant potential electrolysis at −0.20 V. The corresponding current−time and diameter−time correlations are shown in Figure 6.

as postulated in Figure 7. During the initial stages **1** and **2**, the reduction not only proceeds outward but also proceeds downward from the silver wire tip. In addition, the total length and the number of 3PIs both increase with time. After the reduction reaches the bottom of the coating, the total number of 3PIs is fixed but the 3PIs can still propagate radially (or outward), as represented by 3, 4, and 5. Obviously, eqs 1−8 are only applicable to the later stages 4 and 5 when the ratio of $(D_t - D_b)/D_b$ or $(D_t - D_b)/D_t$ is much smaller than 1, which means the length of the top 3PI is negligibly different from that of the bottom 3PI.

During the electrolysis, the image of the back of the AgCl coating was scanned, showing a continuous expansion of the circular gray area which however had a diameter less that 500 μm within the first 40 s; see Figure 8. Since the image was taken on the bottom of the coating which was about 80 μm in thickness, it is then not surprising that the deviation occurred in the first 40 s of the potential step, in agreement with the postulation of Figure 7.

Plotting the average diameter of each circular area, as measured from three or more different angles on an enlarged optical image, against the electrolysis time also resulted in a simple linear correlation, as shown in Figure 6b and predicted by eqs 3 and 4. It should be mentioned that both lines in Figure 6a and b have nonzero intercepts with the vertical axis, while eqs 3 and 4 predict the lines to pass through the origin. This could be due to the initial contact of the wire tip on the coating deviating from an ideal three-phase interpoint.

It should be mentioned that when the light beam of the scanner moved under the electrode tip, a short interruption in current occurred, which is visible on the current−time plots as the small spikes in Figure 6a and also in Figure 9a. However, these interruptions seem to be too small to significantly affect the linear variation of the current against the time after the optical scan.

Effect of Electrode Potentials. The linear correlations shown in Figure 7 were actually observed in a wide range of potentials. Figure 9 displays some examples, for each of which a new contact point was made between the wire tip and the coating. Also, the linear fitting excluded the currents recorded in the initial period when the influence of the difference in length between the top and bottom 3PIs was still large. It can be seen in Figure 9a that the slope of the current−time plot increases with the applied potential. A similar trend is also seen in the diameter−time plots; see Figure 9b. Such potential dependence of the current−time and diameter−time correlations is predicted by eqs 7 and 8.

According to eqs 7 and 8, the logarithm of the ratio of current and time ($V_I = I/t$) or of diameter and time ($V_D = D/t$) should vary linearly with the overpotential or the applied electrode potential. The values of V_I and V_D are actually the slopes of the straight lines in parts a and b of Figure 9, respectively. Indeed, as shown in Figure 10, linear correlations were obtained when the data of different potentials were compared. According to eqs 7 and 8, the slopes of the straight lines in Figure 10a and b are related to αn. For reaction II, $n = 1$, α was found to be

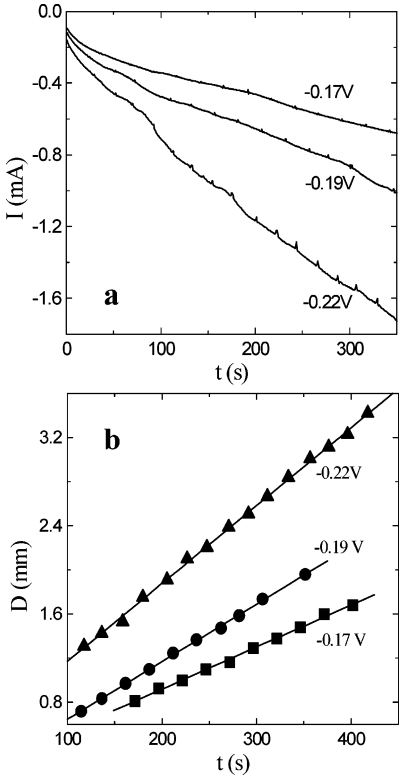

Figure 9. Correlations of (a) the current and (b) the diameter of the reduced area with the electrolysis time at different potentials as indicated.

0.29 ± 0.03 from the two plots. It is worth mentioning that eq 4 can be rearranged to give a linear relationship between V_I and V_D^2, that is, $I/t = V_I = (\pi hnF\rho/2M)V_D^2$. Figure 10c shows the corresponding straight line whose slope allows the calculation of the density of the AgCl coating, ρ, according to eq 4, which was 0.91 g cm^{-3}, indicating a high porosity of the film.

Extrapolating the straight lines in Figure 10a and b to $\eta = 0$ (or $E = E^\circ = 0.03$ V), according to eqs 7 and 8 and using the thickness, h, of the coating as measured by SEM and the density, ρ, of the AgCl coating calculated above, the product of mi_0 was calculated to be $(1.14 \pm 0.31) \times 10^{-4}$ A cm^{-1}, where i_0 is the exchange line current density on the 3PI and m the hypothetic number of parallel circular 3PIs. To make the mi_0 value comparable to the conventional "area" exchange current density on an interface, the ratio mi_0/h may be considered as the exchange area current density through the cross section of the coating. The value of mi_0/h was found to be $(1.42 \pm 0.39) \times 10^{-2}$ A cm^{-2}, which can be compared with that of the reduction of Ag^+ or its complexes (e.g., AgCN and $Ag(CN)_2^-$) in various media, $10^{-3}-10^{-1}$ A cm^{-2}, at the interface between an inert electrode and the electrolyte.[41]

It is worth pointing out that kinetic parameters for solid/solid electrode reactions, such as the Ag/AgCl and other metal/metal salt (insoluble) systems, are rare in the literature. Therefore, the simple thin layer model and the experimental method described here could be a generic technique for obtaining kinetic parameters for electrochemical "solid-to-solid" conversion.

Comparison with the Electroreduction of Solid SiO_2 in Molten $CaCl_2$. Of particular relevance to this work is the previously reported electroreduction of SiO_2 glass by a "point contact electrode"[26] and a "silica sealed tungsten electrode".[27] It was demonstrated that the reduction started at the initial metal/SiO_2/electrolyte 3PI which then propagates along the SiO_2 surface in contact with the molten salt. Following the conversion

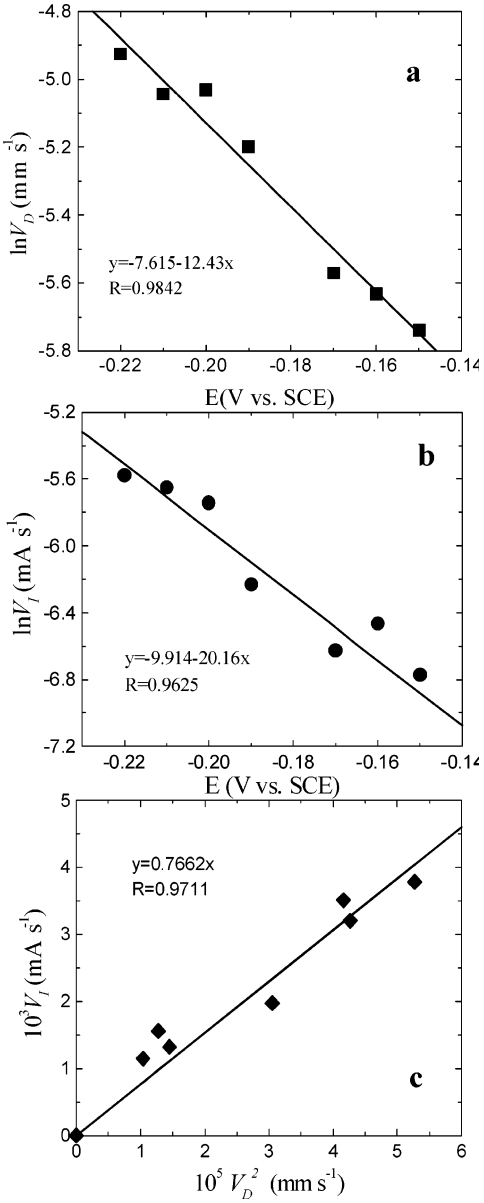

Figure 10. Correlations of the logarithms of the ratios of (a) the diameter of the reduced area and time, $V_D = D/t$, and (b) the current and time, $V_I = I/t$, with the applied electrode potential. In part c is shown the linear correlation between V_I ($=I/t$) and V_D^2 [$=(D/t)^2$] as described by eq 4.

of a thin layer of SiO_2 on the surface to a porous layer of Si, further reduction of the interior of the solid SiO_2 was significantly slowed by diffusion through the porous Si layer.[27] This situation closely resembles the "thin layer model" discussed in previous sections, and a comparison between the two is obviously of both academic interest and industrial importance.

In this work, the silica sealed tungsten electrode or simply $W-SiO_2$ electrode, as shown schematically in Figure 11, was used for both chronoamperometry (constant potential electrolysis) and cyclic voltammetry in molten $CaCl_2$ at 850 °C. In these experiments, a new electrode was always used with either a Pt pseudo- or a quartz sealed Ag/AgCl reference[42] and a graphite crucible counter electrode. For comparison, all potential data given in the later text are converted with reference to the current onset potential on the CV of SiO_2 or simply Si/SiO_2.

During chronoamperometric experiments, the applied potentials were selected according to CVs that were recorded previously[27] or in this work under similar conditions. As shown

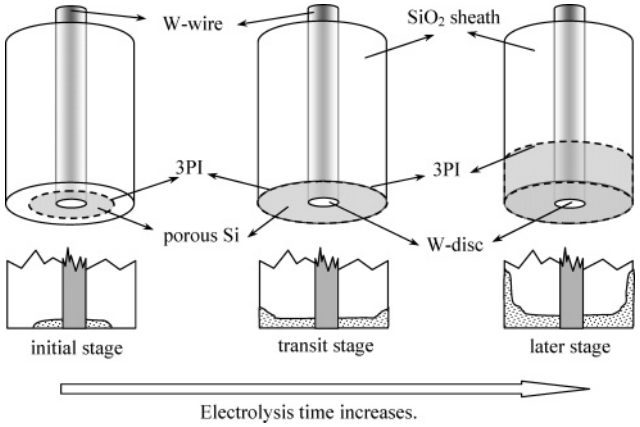

Figure 11. Schematic illustration of the propagation of the Si/SiO_2/electrolyte 3PI along the surface of the $W-SiO_2$ electrode. (3PIs also exist underneath the porous Si layer, but the reduction is restricted by mass diffusion through the porous Si layer.[27]) The diagrams are drawn on the basis of visual and SEM observations of the $W-SiO_2$ electrode at different stages of electroreduction in molten $CaCl_2$ at 850 °C.[27]

by the inset of Figure 12a, the recorded current−time plot exhibited typically three stages: (1) an initial linear increase of the current with time (20−80 s), (2) a slightly sloped current plateau at long times (>200 s), and (3) a transit section connecting stages 1 and 2. The relative length of each of the three sections depended on the applied potential for a given $W-SiO_2$ electrode. While research is still ongoing for a more quantitative understanding, these three features, which were also observed on a different SiO_2 electrode as reported in two recent papers[43,44] (which the authors noticed after submission of this paper), may be qualitatively explained with reference to Figure 11. Initially, the linear increase of the current was due to the electrochemically driven expansion of the Si/SiO_2/electrolyte 3PI along the flat bottom of the $W-SiO_2$ electrode, which is in accordance with our thin layer model. When the 3PI moved over the edge and into the sidewall, its length could not be further increased, resulting in a current plateau (although the increasing resistance of the formed porous Si layer may also contribute). The transition period corresponds naturally to the 3PI propagation over the edge of the $W-SiO_2$ electrode when the situation is different at least in that mass diffusion occurs on both sides of the edge. It should be mentioned that these qualitative explanations are in agreement with visual observations of the electrodes after terminating the experiment at different times.

Three examples of the initial linear current−time relations are presented in Figure 12a. Plotting the logarithms of the slopes, $\ln(I/t) = \ln V_I$, of these straight lines against the applied potentials leads to another approximate linear relationship, as presented in Figure 12b. While this straight line agrees with eq 8, it is also strong evidence that, at least in the initial period, electroreduction on the $W-SiO_2$ electrode follows the thin layer model.

In agreement with the chronoamperometric findings, Figure 13 shows the consecutive CVs recorded on the $W-SiO_2$ electrode and repeats clearly the features of Figure 4, confirming the similarity between the two reduction processes. It is worth mentioning that when the potential was scanned at a faster rate (e.g., 200 mV/s) in a wider range (e.g., 0.5 to −1.0 V), CVs similar to that reported previously were obtained.[27] This implies influences of other factors that are not considered in our thin layer model and will be addressed separately.

It is then decided to estimate the α value according to eq 8. To ensure reliability, further chronoamperometric experiments were performed at potentials in the same range as the CVs in Figure 13. In all cases, linear $\ln V_I - E$ correlations were evident but it was also noticed that the V_I values differed between different sets of measurements; see Figure 12b. In additional to the known experimental variations, it is acknowledged that errors are relatively larger for measurements in the molten salt than for those in water. Nevertheless, from all the obtained data, it was found that $\alpha \approx 10^{-2}$ for $n = 4$. This unusually small α value warrants more discussion on the various kinetic possibilities.

First of all, according to Marcus' microscopic model, α is a function of the reorganization energy, λ, which represents the energy necessary to transform the nuclear configurations in the reactant and the solvent to those of the product state.[2] In comparison with polarization, a large λ value means that it is difficult to change the nuclear configuration and solvation by charge transfer. Hence, the reactant and product are in the same or similar states. In such cases, α is close to 0.5. However, if charge transfer alters nuclear configurations, λ is then comparable to polarization and small α is expected. It is obvious that the nuclear configuration in solid SiO_2 differs from that in solid Si (covalent Si−O bond vs semimetallic Si−Si bond), which agrees with the small α value. In contrast, the Ag atoms have

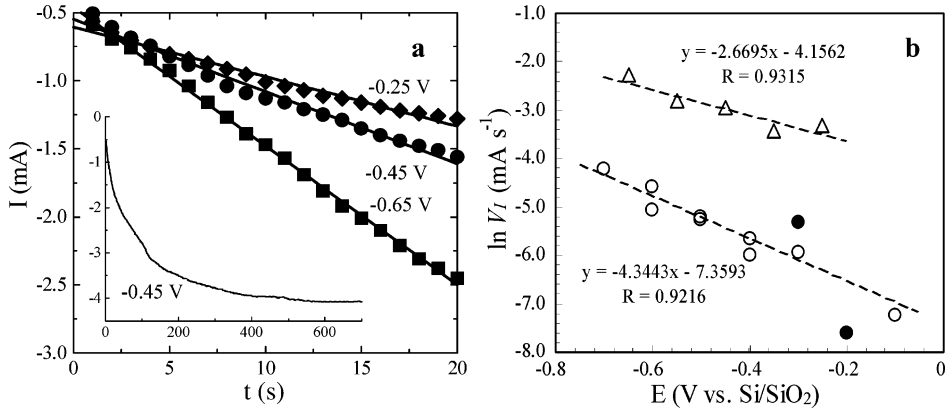

Figure 12. (a) Current−time plots recorded during constant potential electrolysis of the $W-SiO_2$ electrode in molten $CaCl_2$ at 850 °C at different potentials. The inset shows an example of the current−time plot over a longer time. (b) The correlations between the logarithms of the slopes (V_I) of two sets of current−time plots and the applied potentials. The triangles correspond to part a and were obtained in early experiments with the potential being stepped from −0.05 V to the given values. The circles were from later experiments with the potential being stepped from 0.30 V to the given potentials. The fitted straight lines (excluding the two obviously deviating solid circles) are in accordance with eq 8 given in the text, leading to $\alpha = 0.032$ from the triangle data and 0.058 from the circle data for $n = 4$.

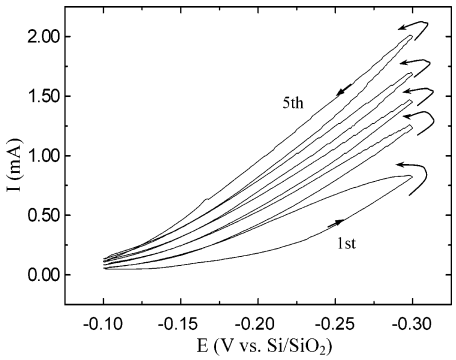

Figure 13. Consecutive cyclic voltammograms in molten $CaCl_2$ (850 °C) of a W−SiO_2 electrode (diameter of W-disk, 300 μm; see Figure 11 for explanation). The arrows indicate the direction of current variation with the potential scan. Scan rate: 5 mV/s.

similar nuclear configurations to that of the Ag^+ ion in both the mainly ionic solid AgCl and the metallic solid Ag, leading to an α value close to 0.5. Second, the electroreduction of AgCl and SiO_2 at the 3PI involves two charge transfer processes: electron between SCP and SMP and anion between SMP and LEP. The results obtained so far do not indicate whether one of the two or both could be in control. Therefore, the measured α value may be apparent in nature. Third, eq 8 is derived on the assumption that the SMP is a conductor, but the resistance of silicon at high temperatures is not insignificant, which may cause deviation in polarization from an electrochemical origin. Last, but not least, the direct predictions of the thin layer model are the linear correlations such as eqs 3 and 4. These predictions agree with the results from this work and from a recent publication.[43] Equations 7 and 8 take the model into a kinetic possibility and are apparently supported by observations in both the AgCl and SiO_2 systems. Nevertheless, research in this laboratory is still ongoing, aiming at a better and more comprehensive understanding of the reduction kinetics of SiO_2 to Si under different experimental conditions, and the results will be published separately.

Conclusion

A simple thin layer model accounting for the electrochemistry at a dynamic solid conductor/solid insulator/liquid electrolyte three-phase interline (3PI) is proposed. The main predictions of the model are well demonstrated using a novel and simple cell that consists of a silver wire in contact with a thin AgCl coating on glass in aqueous KCl electrolyte. The cell also allows in situ observation of 3PI variation following dynamic and static potential perturbations using an optical image scanner. The results show that the expansion of the circular 3PI around the contacting point (or region) proceeds linearly with time but exponentially with the applied potential. In addition, the model allows kinetic information (e.g., the charge transfer coefficient, α) of the electrochemical conversion of solid to solid to be obtained. It also explains very well the consecutive CVs of low scan rates and the initial linear correlations on the chrono-amperometric plots recorded on a SiO_2 sealed W-disk electrode in molten $CaCl_2$.

Acknowledgment. The authors acknowledge gratefully the financial support from the Natural Science Foundation of China (Grant Nos. 20125308 and 50374052). G.Z.C. thanks the Ministry of Education of China for the award of the Cheung Kong Scholarship.

References and Notes

(1) Bockris, J. O'M.; Khan, S. U. M. *Surface Electrochemistry: A Molecular Level Approach*; Plenum: New York, 1993.
(2) Bard, A. J.; Faulkner, L. R. *Electrochemical Methods: Fundamentals and Applications*, 2nd ed.; John Wiley & Sons: New York, 2001.
(3) Chen, X. J.; Khor, K. A.; Chan, S. H. *Solid State Ionics* **2004**, *167*, 379.
(4) Chen, G.; Wei, L.; Luo, J. L.; Sanger, A. R.; Chuang, K. T. *J. Electrochem. Soc.* **2004**, *151*, A232.
(5) Fukui, T.; Ohara, S.; Naito, M.; Nogi, K. *J. Eur. Ceram. Soc.* **2003**, *23*, 2963.
(6) Shkerin, S.; Primdal, S.; Mogensen, M. *Ionics* **2003**, *9*, 140.
(7) Guillet, N.; Rives, A.; Lalauze, R.; Pijolat, C. *Appl. Surf. Sci.* **2003**, *210*, 286.
(8) Brichzin, V.; Fleig, J.; Habermeier, H. U.; Cristiani, G.; Maier, J. *Solid State Ionics* **2002**, *152*, 499.
(9) Lee, H. Y.; Cho, W. S.; Oh, S. M.; Wiemhofer, H. D.; Gopel, W. *J. Electrochem. Soc.* **1995**, *142*, 2659.
(10) Kenjo, T.; Wada, K. *Solid State Ionics* **1994**, *67*, 249.
(11) Wienecke, M.; Bunescu, M. C.; Pietrzak, M.; Deistung, K.; Fedtke, P. *Synth. Met.* **2003**, *138*, 165.
(12) Goprl, W.; Schierbaum, K. D. *Sens. Actuators, B* **1995**, *26*, 1.
(13) Wain, A. J.; Wadhawan, J. D.; Compton, R. G. *ChemPhysChem* **2003**, *4*, 974.
(14) Wain, A. J.; Wadhawan, J. D.; France, R. R.; Compton, R. G. *Phys. Chem. Chem. Phys.* **2004**, *6*, 836.
(15) Wadhawan, J. D.; Wain, A. J.; Kirkham, A. N.; Walton, D. J.; Wood, B.; France, R. R.; Bull, S. D. Compton, R. G. *J. Am. Chem. Soc.* **2003**, *125*, 11418.
(16) Aoki, K.; Tasakorn, P.; Chen, J. Y. *J. Electroanal. Chem.* **2003**, *542*, 51.
(17) Yano, H.; Tanaka, T.; Nakayama, M.; Ogura, K. *J. Electroanal. Chem.* **2004**, *565*, 287.
(18) Yamanaka, I.; Funakawa, A.; Otsuka, K. *J. Catal.* **2004**, *221*, 110.
(19) Marken, F.; Webster, R. D.; Bull, S. D.; Davies, S. G. *J. Electroanal. Chem.* **1997**, *437*, 209.
(20) Schröder, U.; Compton, R. G.; Marken, F.; Bull, S. D.; Davies, S. G.; Gilmour, S. *J. Phys. Chem. B* **2001**, *105*, 1344.
(21) Scholz, F.; Komorsky-Lovrić, Š; Lovrić, M. *Electrochem. Commun.* **2000**, *2*, 112.
(22) Komorsky-Lovrić, Š; Mirèeski, V.; Kabbe, Ch.; Scholz, F. *J. Electroanal. Chem.* **2004**, *566*, 371.
(23) Scholz, F.; Gulaboski, R. *ChemPhysChem* **2005**, *6*, 16.
(24) Xu, P. D., Liu, H. T., Eds. *Lead Acid Battery: Fundamentals and Techniques*; Shanghai Science and Technology Press: Shanghai, 1996.
(25) Chen, G. Z.; Fray, D. J.; Farthing, T. W. *Nature* **2000**, *407*, 361.
(26) Nohira, T.; Yasuda, K.; Ito, Y. *Nat. Mater.* **2003**, *2*, 397.
(27) Jin, X. B.; Gao, P.; Wang, D. H.; Hu, X. H.; Chen, G. Z. *Angew. Chem., Int. Ed.* **2004**, *43*, 733.
(28) Chen, G. Z.; Gordo, E.; Fray, D. J. *Metall. Mater. Trans. B* **2004**, *35*, 223.
(29) Hurless, B. E.; Froes, F. H. *Adv. Mater. Processes* **2002**, *160*, 37.
(30) Hill, S. *New Sci.* **2001**, *170*, 44.
(31) Fenn, A. J.; Cooley, G.; Fray, D.; Smith, L. *Adv. Mater. Processes* **2004**, *162*, 51.
(32) Metcalfe, I. S.; Sundaresan, S. *Chem. Eng. Sci.* **1986**, *4*, 1109.
(33) Bhargava, A.; Francis, A. V.; Biswas, A. K. *J. Colloid Interface Sci.* **1978**, *64*, 214.
(34) McIlroy, D. N.; Alkhateeb, A.; Zhang, D.; Aston, D. E.; Marcy, A. C.; Norton, M. G. *J. Phys: Condens. Matter* **2004**, *16*, R415.
(35) Gordo, E.; Chen, G. Z.; Fray, D. J. *Electrochim. Acta* **2004**, *49*, 2195.
(36) Hasse, U.; Wager, K.; Scholz, F. *J. Solid State Electrochem.* **2004**, *8*, 842.
(37) Hasse, U.; Scholz, F. *Electrochem. Commun.* **2001**, *3*, 429.
(38) Hermes, M.; Scholz, F.: *Electrochem. Communun.* **2000**, *2*, 845.
(39) Ives, D. J. G.; Janz, G. J. *Reference Electrodes: Theory and Practice*; Academic Press: New York and London, 1961.
(40) Scholz, F.; Chen, G. Z. Personal communication.
(41) Bard, A. J., Ed. *Encyclopedia of Electrochemistry of the Elements, Volume VIII*; Marcel Dekker Inc.: New York and Basel, 1978.
(42) Gao, P.; Jin, X. B.; Wang, D. H.; Hu, X, H,; Chen, G. Z. *J. Electroanal. Chem.* **2005**, *579*, 321.
(43) Yasuda, K.; Nohira, T.; Ito, Y. *J. Phys. Chem. Solids* **2005**, 443.
(44) Yasuda, K.; Nohira, T.; Amezawa, K.; Ogata, Y. H.; Ito, Y. *J. Electrochem. Soc.* **2005**, *152*, D69.